Available online at www.sciencedirect.com
ScienceDirect
Mathematics and Computers in Simulation 132 (2017) 120–138
MATHEMATICS AND COMPUTERS IN SIMULATION
www.elsevier.com/locate/matcom

Original articles

Approximation of the differential operators on an adaptive spherical geodesic grid using spherical wavelets

Ratikanta Behera*, Mani Mehra

Department of Mathematics, Indian Institute of Technology Delhi, India

Received 27 May 2014; received in revised form 12 May 2016; accepted 19 July 2016
Available online 25 July 2016

Abstract

In this work, a new adaptive multi-level approximation of surface divergence and scalar-valued surface curl operator on a recursively refined spherical geodesic grid is presented. A hierarchical finite volume scheme based on the wavelet multi-level decomposition is used to approximate the surface divergence and scalar-valued surface curl operator. The multi-level structure provides a simple way to adapt the computation to the local structure of the surface divergence and scalar-value surface curl operator so that the high resolution computations are performed only in regions where singularities or sharp transitions occur. This multi-level approximation of the surface divergence operator is then used in an adaptive wavelet collocation method (AWCM) to solve two standard advection tests, solid-body rotation and divergent flow on the sphere. In contrast with other approximate schemes, this approach can be extended easily to other curved manifolds by considering appropriate coarse approximation to the desired manifold (here we used the icosahedral approximation to the sphere at the coarsest level) and using recursive surface subdivision.

Keywords: Spherical wavelet; Surface divergence operator; Scalar-valued surface curl operator; Spherical geodesic grid; Adaptive wavelet collocation method

1. Introduction

Mathematical modeling of problems in science and engineering (e.g. weather forecast, climate modeling, physical science and medical imaging) typically involves solving partial differential equations (PDEs) on the sphere. On the other hand, most of these problems have localized structures or sharp transitions, which might occur intermittently anywhere on the spheres or change their locations and scales in space and time. Furthermore, most PDEs of mathematical physics and engineering can be formulated in terms of fundamental differential operators, such as divergence, gradient, Laplacian, Jacobian and curl operators. Researchers have shown that the best approximate solution of these types of PDEs by approximating the fundamental operators in efficient way, but approximating these operators on uniform grids is impractical, since high-resolution computations are required only in regions where sharp transitions occur [42,44].

* Corresponding author.
E-mail addresses: ratikanta.behera@imag.fr (R. Behera), mmehra@maths.iitd.ac.in (M. Mehra).

http://dx.doi.org/10.1016/j.matcom.2016.07.007

It is necessary to construct a grid over the sphere for approximating differential operators. In particular, we consider an icosahedral grid. Various grid construction methods based on recursive subdivision of the icosahedron have been proposed by Sadourny et al. [35], Williamson [46] and Masuda and Ohnishi [21]. Many researchers have already utilized such geodesic grids [17,30]. The main reason for the choice of this grid is its quasi-uniform convergence of the sphere, which solves automatically the pole problem of the regular latitude–longitude grid [8]. Many studies concern the development of finite difference and finite volume approximation using various geodesic grids [21,40]. However, the geodesic grid has been regularized by applying a spring dynamics adjustment or smoothing based on the iteration of Laplace–Beltrami operator [31,40], which leads to a significant improvement of the accuracy of the representation of the differential operators. Nevertheless, these approaches are still non-adaptive.

Adaptive wavelet based method has been developed in the past aiming at a speed up of classical numerical discretization methods (finite differences or finite volumes) by locally adapting the grid to the solution which can then result in significant memory reduction. The main advantage of the adaptive wavelet method, when compared to conventional (non-wavelet) numerical methods, is that they use far fewer grid points than the other method when applied to problems with a great diversity of spatial–temporal scales [43]. Therefore adaptivity provides an enormous potential for advancing the frontiers of computability. The adaptive wavelet methods have been discussed in various contexts for flat geometries [33,34,41]. Recently, the adaptive wavelet methods have been extended from flat geometries to a spherical geometry by Mehra and Kevlahan [25]. Furthermore, a multi-level adaptive wavelet based method for the representation of the Laplace–Beltrami, Jacobian and gradient operators on the sphere has been developed recently [7,24,25]. The prowess and computational efficiency of these operators are demonstrated for the solution of advection, diffusion equations and barotropic vorticity equation on the sphere [5,6,25].

The purpose of this paper is to propose a multi-level approximation of the differential operators on an adaptive spherical geodesic grid and showing results from the standard advection tests, solid-body rotation and divergent flow on the sphere. As we are solving problems arising from atmospheric physics, meteorology and climatology context, conservation of physical quantities – e.g., global mass – in flux computations is of special interest. For the evaluation of the numerical fluxes on the locally refined grid we devise a wavelet approximation scheme without increasing significantly the number of costly flux evaluations.

The numerical simulation in a divergent flow environment is more complex than the non-divergent case. Furthermore, when the solution of these flow problems are highly localized in position and scale, we need efficient approximation of the divergence operator to solve these problems. But these types of problems have been solved previously [27] on non-adaptive grid. Our multi-level approximation of the surface divergence operator on an adaptive spherical geodesic grid provides local grid refinement and error control. Thus multi-level approximation of the surface divergence operator is then used in an AWCM to solve these types of problems.

The main objective of this paper is to apply a multi-level approximation of the differential operator on an adaptive spherical geodesic grid. Furthermore, the definitions of the discrete approximations of the differential operators presented in the following hold in any coordinate system because they involve only geometrical quantities such as length, area, and volumes and use coordinate invariant components of the vectors. Thus the strength of this approximation scheme is that it can be extended easily to other curved manifolds by considering an appropriate coarse approximation of the desired manifold. Here we used the icosahedral approximation of the sphere at the coarsest level. Hence the proposed approximation technique can allow the climate modeling community to perform large scale simulations of atmosphere and ocean dynamics.

The outline of the paper is as follows. In Section 2 we introduce the construction of the wavelets on the spherical geodesic grid system. The multi-level adaptive wavelet approximation of surface differential operators on the spherical geodesic grid is presented in Section 3. We discuss the numerical result of both operators by taking two test cases and the multi-level adaptive wavelet approximation of surface divergence operator is applied to simulate two test problems: (1) solid body rotation of a cosine bell, and (2) a divergent flow over the sphere in Section 4. Finally, the proposed development has been summarized in Section 5 with a brief discussion on further research in this direction.

2. Wavelets on the sphere

The extension of wavelet analysis to a spherical geometry is of important theoretical and practical interest for an accurate and efficient numerical solution of PDEs or data set on the sphere. Several wavelet transforms on the spherical geometry have been proposed in recent years and their performance depends on the application. Holschneider [18] was

the first to build a genuine spherical continuous wavelet transform, but it contains a parameter that although interpreted as a dilation parameter it is difficult to compute. A satisfactory extension of the continuous spherical wavelet transform based on a group theoretical approach was defined by Antoine and Vandergheynst [1,2]; however, this construction is derived entirely from group theoretic principles and inherently satisfies a number of natural requirements. A number of works construct a solution using a harmonic approach [16,29]; however, these solutions suffer from the poor localization of the spherical harmonic functions.

Traditionally, wavelet-based numerical methods make use of first generation wavelets that are constructed by discrete (typically dyadic) dilation and translation of a single mother wavelet $\psi(x)$. This results in creation of first generation wavelets [11,12], that are defined either in infinite or periodic domains. The Fourier transform is the primary tool used in the construction of most of the first-generation wavelet bases. There are few first-generation wavelets that can be constructed without the use of Fourier techniques [10]. For example, interpolating wavelets [13]. However, the wavelet basis constructed using interpolating scaling functions [42] does not provide a Riesz basis for L_2, as the wavelet itself has non-zero mean, and the dual wavelets are Dirac δ-functions which do not belong to L_2. The second generation wavelets based on a lifting scheme [38,39] were introduced to eliminate the restrictions and deficiencies of first generation wavelets. The lifting scheme provides users with much flexibility for building second generation wavelets bases with prediction and update coefficients. The details of the second generation lifting scheme are described in [38,39].

Among these above spherical wavelet transforms the second generation wavelet based spherical wavelet transform has attracted much attention in last few years [39]. The basic philosophy behind second generation wavelets is to build wavelets with all desirable properties (localization, fast transform) adapted to much more general settings than the real line. The notion that a basis function can be written as a finite linear combination of basis functions at a finer, more subdivided level, is maintained and forms the key behind the fast transform. Second generation wavelet based method for the representation of the Laplace–Beltrami, Jacobian and gradient operators on the sphere [7,24,25] has been developed recently. Many other papers [5,6,24] have already utilized such operators to solve PDEs on the sphere.

2.1. The model grid on the sphere

A number of continuous representation of wavelet on sphere have been proposed in recent years that also have exact discretization, for example needlets [3,20,28], scale-discretized wavelets [45] and isotropic pyramidal wavelets [37]. In addition, a number of discrete constructions, also based on the lifting scheme of Sweldens, have also been developed in the field of cosmology [4,22,23]. These are based on the HEALPix discretization of the sphere. However, this implementation is restricted to an equiangular tessellation of the sphere and the pixels of an equiangular tessellation are densely spaced about the poles. To avoid these problems, quasi-uniform triangulations are gaining popularity in the climate modeling community. These almost uniform spherical triangular grids are the fundamental idea behind second generation spherical wavelets. Specifically, the grid used here is very similar to the simple twisted icosahedral grid described by Heikes and Randall [17]. In general, the icosahedron is recursively refined by bisecting edges of the existing grid (i.e. dyadic refinement). However, for large numbers of subdivisions (e.g. greater than 8 or 9) the grid becomes increasingly non-uniform which can lower the convergence rate of interpolation on the grid. This would not be the case for the HEALPix scheme, for which pixels are of equal area. To correct this non-uniformity the grid points can be redistributed, or the interpolation and differential operators on the grid can be modified [17].

To construct a spherical geodesic grid (also called icosahedral–hexagonal grid), we begin with a platonic solid (see Fig. 1), which has spherical triangular faces, then with help of a subdivision scheme one can get new vertices onto the surface of the sphere. Here we consider only the simplest edge bisection method for which the number of grid points at subdivision level j is $\mathcal{K}^j = 10 \times 4^j + 2$. Each of the $\mathcal{K}^j$ grid points is surrounded by 6 nearest neighbors except for the original 12 icosahedral vertices which have 5 nearest neighbors (see Fig. 1).

Let $\mathcal{S}$ be a triangulation of the sphere S and denote the set of all vertices obtained after subdivisions with $\mathcal{S}^j = \{p_k^j \in S | k \in \mathcal{K}^j\}$, where $\mathcal{K}^j$ is an index set, and let q_k^j be the center of the triangle p_i^j, p_k^j, p_{k+1}^j (see Fig. 2). Now the original platonic solid icosahedral $\mathcal{S}^0$ contains only 12 vertices (see Fig. 1(a)) and the $\mathcal{S}^1$ contains those vertices and all new vertices on the edge midpoints (see Fig. 1(b)). Since $\mathcal{S}^j \subset \mathcal{S}^{j+1}$ we also let $\mathcal{K}^j \subset \mathcal{K}^{j+1}$. Let $\mathcal{M}^j = \mathcal{K}^{j+1}/\mathcal{K}^j$ be the indices of the vertices added when going from level j to $j+1$ (see Fig. 1).

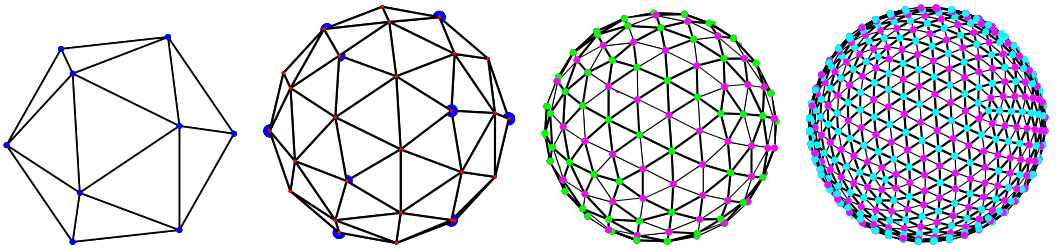

(a) Level-0. (b) Level-1. (c) Level-2. (d) Level-3.

Fig. 1. Geodesic grid generation based on an icosahedron embedded in the sphere.

2.2. Multi-scale decomposition

A second generation multi-resolution analysis (MRA) [39] of the sphere provides a sequence $\mathcal{V}^j \subset L_2(S)$ with $j \geqslant 0$ and the sphere $S = \{p = (p_x, p_y, p_z) \in \mathbb{R}^3 : \|p\| = a\}$, where a is the radius of the sphere.

- $\mathcal{V}^j \subset \mathcal{V}^{j+1}$,
- $\bigcup_{j\geq 0} \mathcal{V}^j$ is dense in $L_2(S)$,
- Each $\mathcal{V}^j$ has a Riesz basis of scaling functions $\{\phi_k^j | k \in \mathcal{K}^j\}$.

Since $\phi_k^j \in \mathcal{V}^j \subset \mathcal{V}^{j+1}$, for every scaling function ϕ_k^j there is a unique set of filter coefficients $\{h_{k,l}^j\}$ such that

$$\phi_k^j = \sum_{l \in \mathcal{K}^{j+1}} h_{k,l}^j \phi_l^{j+1}. \tag{1}$$

Note that the filter coefficients $\{h_{k,l}^j\}$ can be different for every $k \in \mathcal{K}^j$ at a given level $j \geqslant 0$. Therefore each scaling function satisfies a different refinement relation (i.e. unlike first generation wavelets there is no unique mother wavelet). Each MRA is accompanied by a dual MRA consisting of nested spaces $\tilde{\mathcal{V}}^j$ spanned by the dual scaling functions $\tilde{\phi}_k^j$, which are bi-orthogonal to the scaling functions:

$$\langle \phi_k^j, \tilde{\phi}_{\acute{k}}^j \rangle = \delta_{k,\acute{k}}, \quad \text{for } k, \acute{k} \in \mathcal{K}^j, \tag{2}$$

where $\langle f, g \rangle = \int_s fg dw$ is the inner product on the sphere. The dual scaling functions satisfy refinement relations with coefficients $\{\tilde{h}_{k,l}^j\}$.

Wavelet coefficients encode the difference between two successive levels of representation (i.e. the details between the fine representation and the coarse representation of a function at two adjacent scales), i.e. wavelets form a Riesz basis for the space $\mathcal{W}^j$, which is the complement of $\mathcal{V}^j$ in $\mathcal{V}^{j+1}$ (i.e. $\mathcal{V}^{j+1} = \mathcal{V}^j \bigoplus \mathcal{W}^j$). In our case, the wavelets form a Riesz basis for $L_2(S)$ and allow a function to be represented by its wavelet coefficients. Since $\mathcal{W}^j \subset \mathcal{V}^{j+1}$, we can write

$$\psi_k^j = \sum_{l \in \mathcal{K}^{j+1}} g_{k,l}^j \phi_l^{j+1}, \tag{3}$$

where $g_{k,l}^j$ are the wavelet coefficients and the spherical wavelets [36] ψ_m^j have $\tilde{d}$ vanishing moments, if there exist $\tilde{d}$ linearly independent polynomials $P_i, 0 \leqslant i < \tilde{d}$ such that

$$\langle \psi_m^j, P_i \rangle = 0 \quad \text{for all } j \geqslant 0, m \in \mathcal{M}^j, \tag{4}$$

where $\mathcal{M}^j$ is the index set and polynomials P_i are on $\mathbb{R}^3$ restricted to the sphere. The main advantage of the wavelet decomposition is its ability to provide a compressed representation of a large class of functions. For functions which contain isolated small scales on a large scale background, most of the wavelet coefficients are small. Discarding them and reconstructing with the remaining coefficients provide an efficient multi-scale decomposition of the original function.

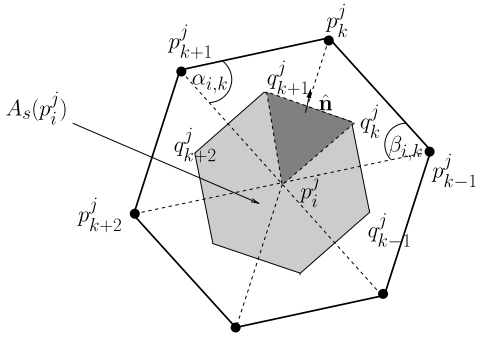

Fig. 2. Schematic figure of angles $\alpha_{i,k}, \beta_{i,k}$, where $\alpha_{i,k}, \beta_{i,k}$ are angles of $p_i^j\, p_{k+1}^j p_k^j$ and $p_i^j\, p_{k-1}^j p_k^j$ respectively. Further, $\hat{\mathbf{n}}$ is the outward pointing unit normal vector of an edge $q_k^j q_{k+1}^j$.

3. Multi-level wavelet approximation

The approximation of the differential operators (surface divergence and scalar-valued surface curl operator) has been performed on uniform grids using finite volumes approach [32,40] on the surface of the sphere. Here the multi-level wavelet approach provides a natural framework to represent differential operators with significantly fewer degrees of freedom, while still retaining a good approximation. Here we consider a sphere of radius a parametrized in terms of spherical coordinates (θ, ϕ), where θ $(-\pi \leqslant \theta \leqslant \pi)$ and ϕ $(-\pi/2 \leqslant \phi \leqslant \pi/2)$ are the longitude and latitude respectively.

3.1. Differential operators

Multi-level approximation of the surface gradient operator, Jacobian operator, Laplace–Beltrami operator on an adaptive spherical geodesic grid has been developed [5,7,25]. Further, the approximation of the Laplace–Beltrami operator on an optimal adaptive spherical geodesic grid has been developed by Mehra and Kevlahan in [24]. Here, we focus only on the approximation of surface divergence and scalar-valued surface curl operator on an adaptive spherical geodesic grid by use of spherical wavelets.

3.1.1. Surface divergence operator

The divergence operator on the surface of the sphere is given by

$$\vec{\nabla} \cdot \vec{\mathbf{V}} = \frac{1}{a \cos\phi} \left[\frac{\partial u}{\partial \theta} + \frac{\partial v \cos\phi}{\partial \phi} \right], \tag{5}$$

where $\vec{\mathbf{V}}$ is the smooth vector field on $\mathcal{S}$ with values in $\mathcal{T}\mathcal{S}$ (tangent space), $\hat{\theta}$ and $\hat{\phi}$ are the unit vectors in the direction of longitude and latitude respectively. Let $\mathcal{S}^j$ be the region on the sphere bounded by ∂s. Then by definition of surface divergence operator is

$$\nabla \cdot \vec{\mathbf{V}} = \lim_{A_s \to 0} \frac{1}{A_s} \int_{\partial s} \vec{\mathbf{V}} \cdot \hat{\mathbf{n}} ds, \tag{6}$$

where A_s is the area of the one ring neighborhood given by [26] and $\hat{\mathbf{n}}$ is the outward pointing unit normal field of the boundary ∂s. Let p_i^j be a vertex of the triangulation at level j and $p_k^j, k \in N(i)$ be the neighboring vertices of p_i^j (see Fig. 2). Now if any arbitrary smooth vector $\vec{\mathbf{V}}$ at q_k^j is calculated by

$$\vec{\mathbf{V}}(q_k^j) = \frac{\vec{\mathbf{V}}(p_i^j) + \vec{\mathbf{V}}(p_{k-1}^j) + \vec{\mathbf{V}}(p_k^j)}{3}. \tag{7}$$

Let us consider l_k to be the length of the arc between center of triangle q_k to center of triangle q_{k+1}, and $\hat{\mathbf{n}}_k$ is the unit vector direction perpendicular to l_k, and points outward relative to cell center q_k^j. The outward flux crossing over

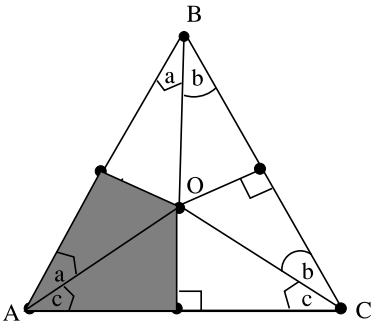

Fig. 3. One ring neighbors angles on a non-obtuse triangle.

the edge $q_k q_{k+1}$ is written as

$$f_k = l_k \frac{\vec{\mathbf{V}}(q_k^j) + \vec{\mathbf{V}}(q_{k+1}^j)}{2} \cdot \hat{\mathbf{n}}_k. \tag{8}$$

Then one can approximate the surface divergence operator on a spherical geodesic grid as follows

$$\nabla \cdot \vec{\mathbf{V}}(p_i^j) = \frac{1}{A_{\mathcal{S}}(p_i^j)} \sum_{k \in N(i)} l_k \left[\frac{\vec{\mathbf{V}}(q_k^j) + \vec{\mathbf{V}}(q_{k+1}^j)}{2} \right] \cdot \hat{\mathbf{n}}_k \tag{9}$$

where $A_s(p_i^j)$ is the area of one-ring neighborhood. For computing one-ring neighborhood, consider a non-obtuse triangle A, B, C with circumcenter O, as depicted in Fig. 3, now we compute the one-ring for A. Using the properties of perpendicular bisectors, one can find: $a + b + c = \pi/2$, and therefore, $a = \pi/2 - \angle B$ and $c = \pi/2 - \angle C$. The one-ring neighborhood for point A lies within this triangle if the triangle is non-obtuse, and is thus: $\frac{1}{8}(|AC|^2 \cot \angle B + |AB|^2 \cot \angle C)$. Summing these areas for the whole one-ring neighborhood, one can write the area for a vertex p_i^j as a function of the neighbors p_k^j:

$$A_s(p_i^j) = \frac{1}{8} \sum_{k \in N(i)} (\cot \alpha_{i,k} + \cot \beta_{i,k}) \, ||p_k^j - p_i^j||^2, \tag{10}$$

where $\alpha_{i,k}$ and $\beta_{i,k}$ are the angles shown in Fig. 2 and $N(i)$ is the set of nearest neighbor vertices of vertex p_i^j. A procedure for computation of cotangent function and approximation of Laplace–Beltrami operator is explained in [26]. Further an approximation of the Laplace–Beltrami operator on an adaptive and optimal adaptive spherical geodesic grid is described in [24,25].

3.1.2. Scalar-valued surface curl operator

The scalar-valued curl operator on the surface of the sphere is given by

$$\hat{\mathbf{k}} \cdot (\vec{\nabla} \times \vec{\mathbf{V}}) = \frac{1}{a \cos \phi} \left[\frac{\partial v}{\partial \theta} - \frac{\partial u \cos \phi}{\partial \phi} \right]. \tag{11}$$

Here $\hat{\mathbf{k}}$ is the vertical unit vector to the surface of the sphere. The alternative form of the definition of the scalar-valued surface curl operator is

$$\hat{\mathbf{k}} \cdot (\vec{\nabla} \times \vec{\mathbf{V}}) = \left(\lim_{A_s \to 0} \frac{1}{A_s} \int_{\partial s} \hat{n} \times \vec{V} ds \right) \cdot \hat{\mathbf{k}}. \tag{12}$$

Then one can approximate scalar-valued surface curl operator on a spherical geodesic grid as follows

$$\hat{\mathbf{k}} \cdot \vec{\nabla} \times \vec{\mathbf{V}}(p_i^j) = \left[\frac{1}{A_s(p_i^j)} \sum_{k \in N(i)} l_k \hat{\mathbf{n}}_k \times \left(\frac{\vec{\mathbf{V}}(q_k^j) + \vec{\mathbf{V}}(q_{k+1}^j)}{2} \right) \right] \cdot \hat{\mathbf{k}}. \tag{13}$$

The major strength of second generation wavelet based techniques is their ability to adapt the computational grid according to the approximations of spherical differential operators. In second generation wavelet based techniques every wavelet is uniquely associated with a computational grid point, and thus grid adaptation is simply based on the analysis of these wavelet coefficients, i.e., the computational grid consists of points corresponding to wavelets whose coefficients are greater than a given threshold (a parameter that controls the accuracy of the differential operator). With this beautiful technique of second generation wavelet, a differential operator is obtained on a near optimal grid for a given accuracy. We have discussed in the next subsection that the adaptation of the computational grid does not require additional effort and consists merely in turning on and off wavelets at different locations and scales. Furthermore, grid adaptation is achieved by analyzing the differential operator and not necessary any *ad hoc* assumptions.

3.2. Approximation of differential operators on an adaptive grid

Grid adaption occurs quite naturally in wavelet methods, e.g. [33,34,41] for flat geometries, it has been also extended from flat geometries to a spherical geometry [25]. The proposed adaptive multi-level approximation of surface divergence and scalar-valued surface curl operators achieves accuracy and computational efficiency on a recursively refined spherical geodesic grid. The order of accuracy of the overall multi-level approximation of the differential operators is same as the finite volume scheme used by Tomita et al. [40]. Further, the multi-level structure provides a simple way to adapt the computation to the local structure of the differential operators. Let us consider the multi-scale decomposition of a function $u(p) \in L_2(S)$ at a certain level of resolution $j \geq J_0$, where J_0 is the coarse level decomposition.

$$u(p) = \sum_{k \in \mathcal{K}^0} c_k^{J_0} \phi_k^{J_0}(p) + \sum_{j=J_0}^{\infty} \sum_{m \in \mathcal{M}^j} d_m^j \psi_m^j(p). \tag{14}$$

This equation can be written as sum of two terms composed of wavelets whose coefficients are respectively above and below some prescribed threshold ϵ, i.e.

$$u(p) = u_{\geq}(p) + u_{<}(p), \tag{15}$$

$$\text{where} \quad u_{\geq}(p) = \sum_{k \in \mathcal{K}^0} c_k^{J_0} \phi_k^{J_0}(p) + \sum_{j=J_0}^{\infty} \sum_{\substack{m \in \mathcal{M}^j \\ |d_m^j| \geq \epsilon}} d_m^j \psi_m^j(p), \tag{16}$$

$$u_{<}(p) = \sum_{j=J_0}^{\infty} \sum_{\substack{m \in \mathcal{M}^j \\ |d_m^j| < \epsilon}} d_m^j \psi_m^j(p), \tag{17}$$

where J_0 is the coarse level of approximation, discarding the collocation points associated with wavelet coefficients less than prescribed threshold ϵ, an irregular collocation grid $\mathcal{V}_s$ of significant points can be defined.

$$\mathcal{V}_s = \left\{ p_k^0 \bigoplus \bigcup_{j>0} p_k^j : k \in \mathcal{K}_0^j \right\}, \quad \text{where } \mathcal{K}_0^j = \{k \in \mathcal{K}^j : |d_k^j| \geq \epsilon\}. \tag{18}$$

Collocation points on the coarsest level, p_k^0, are associated only with scaling functions and are always in $\mathcal{V}_s$. We define the total number of significant points in $\mathcal{V}_s$: $\mathcal{N} = \dim \mathcal{V}_s$. Donoho [13] has shown that for smooth enough u,

$$\|u - u_{\geq}\|_{\infty} \leq c_1 \epsilon, \tag{19}$$

and the number of significant coefficients $\mathcal{N} = N(\epsilon)$ depends on ϵ,

$$N(\epsilon) \leq c_2 \epsilon^{-n/d}, \tag{20}$$

where d is the order of interpolation, n is the dimension of the problem and the coefficients c_i, where $i = 1, 2, 3$ depend on the function. Combining relations (19) and (20) gives the following error bound in terms of $N(\epsilon)$,

$$\|u - u_{\geq}\|_{\infty} \leq c_3 N(\epsilon)^{-d/n}. \tag{21}$$

Note that d controls the number of zero moments of the interpolating scaling function. This error estimate has been verified numerically for flat geometry [41,42] and on the sphere [25]. The estimates (19)–(21) allow us to control both the error of the approximation and the number of wavelet coefficients (i.e. grid points) using only the threshold parameter ϵ. In the present case we use butterfly interpolation [14,36], which should give fourth-order convergence $d = 4$ provided the grid is sufficiently uniform (i.e. for a moderate number of refinement levels). For very large numbers of the levels the convergence rate of the butterfly interpolation drops to second-order accuracy, $d = 2$, as the bisection refinement leads to a distorted grid near the edges and vertices of the original icosahedron.

Here the goal consists in performing the differential operator by finite volume method described above in a more economic fashion, by taking into account local regularity information about the current approximation. Assume that we perform local differentiation at a point $p_k^j \in \mathcal{S}^j$ and h^j is the quantity describing the local grid spacing in all directions at that point. Then by construction it follows that the local truncation error of interpolation scheme is $(h^j)^d = O(\epsilon)$. Then approximation of surface divergence and scalar-valued surface curl operator will reduce the order of the scheme by 1 and make it $(h^j)^{d-1} = O(\epsilon^{d-1/d})$.

Let us consider $\mathcal{D}$ is the differential operator either $(\nabla\cdot\vec{\mathbf{V}})$ or $(\vec{\mathbf{K}}\cdot\vec{\nabla}\times\vec{\mathbf{V}})$. The convergence rate of the approximation of differential operator is $\mathcal{D}_{\geq}$ on the adapted spherical grid to the approximation of the differential operator on the full spherical grid $\mathcal{D}$ is given by

$$\|\mathcal{D} - \mathcal{D}_{\geq}\|_\infty \leq c_5\epsilon^{1-1/d} \leq c_6 N(\epsilon)^{-(d-1)/2}. \tag{22}$$

Note that this convergence rate measures the error due to the wavelet filtering on the adaptive grid when the grid is adapted by filtering the function u (hence the fact that the error is no longer proportional to ϵ). As mentioned above, we use butterfly interpolation and so we expect that $\|\mathcal{D} - \mathcal{D}_{\geq}\|_\infty \sim \epsilon^{3/4} \sim N(\epsilon)^{3/2}$ for sufficiently uniform grids, and $\|\mathcal{D} - \mathcal{D}_{\geq}\|_\infty \sim \epsilon^{1/2} \sim N(\epsilon)^{1/2}$ for non-uniform grids (i.e. when using a very large number of refinement levels).

In order to benefit from the wavelet compression, we need to be able to reconstruct these operators $(\nabla\cdot\vec{\mathbf{V}})_{\geq}(p)$ and/or $(\vec{\mathbf{K}}\cdot\vec{\nabla}\times\vec{\mathbf{V}})_{\geq}(p)$ from the subset of $\mathcal{N}$ grid points (recall Eq. (22)). Again we recall that the wavelet coefficients measure the local differences between approximations of a function at two successive levels of resolution j and $j+1$. Thus, if there are no points in the immediate vicinity of a grid point p_i^j (i.e. $d_k^j \leq \epsilon$ for all $k \in N(i)$, and the points $p_i^j, k \in N(i)$, are not present in $\mathcal{S}^{j+1}$) then there exists some neighborhood Ω_i^j of p_i^j, where the function can be interpolated by a wavelet interpolant based on $s_{k,m}^j (k \in \mathcal{K}_m)$ to accuracy $O(\epsilon)$,

$$\left| u(p) - \sum_{k\in\mathcal{K}(i)} s_{k,m}^j \phi_k^j(p) \right| \leq c_3\epsilon, \tag{23}$$

where the coefficients $s_{k,m}^j$ can be chosen as presented in [25]. The grid adaptation algorithm for surface divergence and scalar-valued surface curl operator is described in Algorithm 1. The application of this algorithm is illustrated in the following test cases.

4. Results and discussion

In order to test the multi-level approximation of surface divergence operator and scalar-valued surface curl operator on an adaptive spherical geodesic grid, we have considered two test cases. For first test case we have used the test function introduced by Heikes and Randall [17] and for the second test case we have considered a Gaussian function on the sphere. In both the cases we have to approximate surface divergence $(\nabla\cdot\vec{\mathbf{V}})$ and scalar-valued surface curl $(\hat{\mathbf{k}}\cdot(\nabla\times\vec{\mathbf{V}}))$ operators using the algorithm mentioned in this section. Numerical errors are estimated using L_∞ norm, where L_∞ norm is computed by

$$\|\mathcal{D}\|_\infty = \max_{k\in\mathcal{K}^j}(|\mathcal{D}(p_k^j)|). \tag{24}$$

The rest of the section is organized as follows. In the first two consecutive subsections, two test functions were taken to verify multi-level adaptive wavelet approximation of surface divergence and scalar-valued surface curl operator on the sphere. Furthermore, in the next subsection we use approximation of surface divergence operator to solve advection

Algorithm 1: GRID ADAPTATION OF THE SURFACE DIVERGENCE AND SCALAR-VALUED SURFACE CURL OPERATOR.

Choose parameters:

- A coarsest level J_0 and a threshold parameter $\epsilon > 0$
- Positive adjacent zone constants M and L

Iterative grid adaptation:
m = 0
$\mathcal{S}_{,\geq} = \mathcal{S}^{J_0}$
while $m = 0$ or $\mathcal{S}_{\geq,m} \neq \mathcal{S}_{,m-1}$ $||\mathcal{D} - \mathcal{D}_{\geq,m}||_\infty > \epsilon$ **do**
  Sample consider a differential operator $\mathcal{D}$ on $\mathcal{S}_{\geq,m}$ to give $\mathcal{D}_{\geq,m}$.
  m = m+1
  Forward wavelet transform
  Compression: retain only signification coefficient $|d_k^j| \geq \epsilon$ to initialize $\mathcal{S}_{\geq,m}$.
  Reconstruction check: (described in [25])
    add grid points needed to calculate significant coefficients.
    add all points at coarsest level: $\mathcal{S}^{J_0} \subset \mathcal{S}_{\geq,m}$.
  Adaptation: add grid points associated with adjacent zone.
  Inverse wavelet transform: interpolates $\mathcal{D}_{\geq,m}$ onto new grid $\mathcal{S}_{\geq,m}$.
Converged result: $\mathcal{S}_\geq = \mathcal{S}_{\geq,m}$, $\mathcal{D}_\geq = \mathcal{D}_{\geq,m}$.

equations on the sphere, here the aim is to check the multi-level approximation of surface divergence operator more rigorously.

Test case-1

As proposed by Heikes and Randall [17], we have used the test vector function $\vec{\mathbf{V}}$, such that $\vec{\mathbf{V}} = \alpha\nabla\beta$, where $\alpha(\theta, \phi) = \sin\theta$, and $\beta(\theta, \phi) = \cos\theta\cos^4\phi$. Hence

$$\begin{aligned}\vec{\mathbf{V}} &= \hat{\theta}v_1 + \hat{\phi}v_2,\\ &= \hat{\theta}(-\cos^3\phi\sin^2\theta) + \hat{\phi}(-\cos^3\phi\sin\phi\sin\theta\cos\theta).\end{aligned} \tag{25}$$

Test case-2

For this test case we consider a localized Gaussian function on the sphere

$$\begin{aligned}\vec{\mathbf{V}} &= \hat{\theta}v_1 + \hat{\phi}v_2\\ &= \hat{\theta}\exp\left[-\frac{(\theta-\theta_0)^2 + (\phi-\phi_0)^2}{L^2}\right] + \hat{\phi}\exp\left[-\frac{(\theta-\theta_1)^2 + (\phi-\phi_1)^2}{L^2}\right],\end{aligned} \tag{26}$$

where $\theta_0 = 0$, $\phi_0 = 0$, $\theta_1 = 0.5$ and $\phi_1 = 0.5$ and $L = 1/2\pi$.

4.1. Adaptive approximation of surface divergence operator

The approximation of the surface divergence operator of test case-1 is shown in Fig. 4 (left) and its adaptive computational grid $(\nabla\cdot\vec{\mathbf{V}})_\geq(p)$ is presented in Fig. 4 (right). In the same way the approximation of surface divergence operator of test case-2 is shown in Fig. 5 (left) and its adaptive computational grid $(\nabla\cdot\vec{\mathbf{V}})_\geq(p)$ is presented in Fig. 5 (right). Hence the grid is fine only in regions where the function has a strong gradient. Therefore, adaptive grids are capturing, identifying, and analyzing local structures of these problems.

The relation between $\|(\nabla\cdot\vec{\mathbf{V}}) - (\nabla\cdot\vec{\mathbf{V}})_\geq\|_\infty$ and ϵ is represented in Fig. 6 (test case-1 and test case-2 left and right respectively), which is compared to the theoretical prediction (22) for fourth-order butterfly interpolation derived in

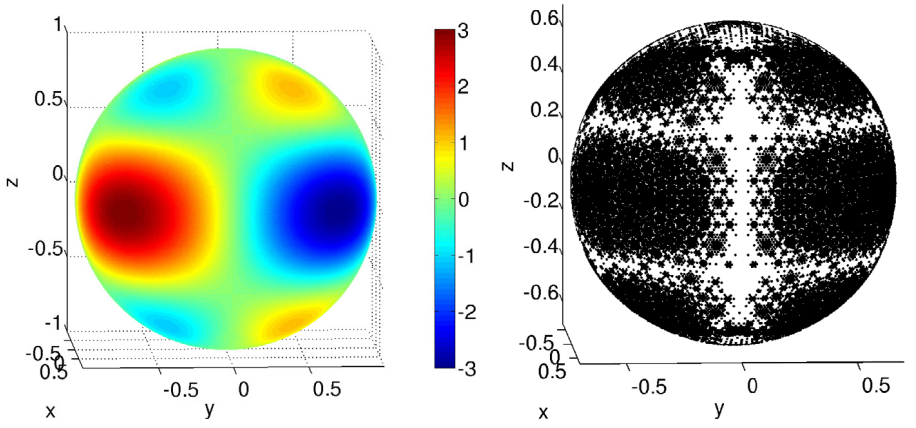

Fig. 4. Approximation of surface divergence operator of test case-1 (left) and its adaptive grid (right).

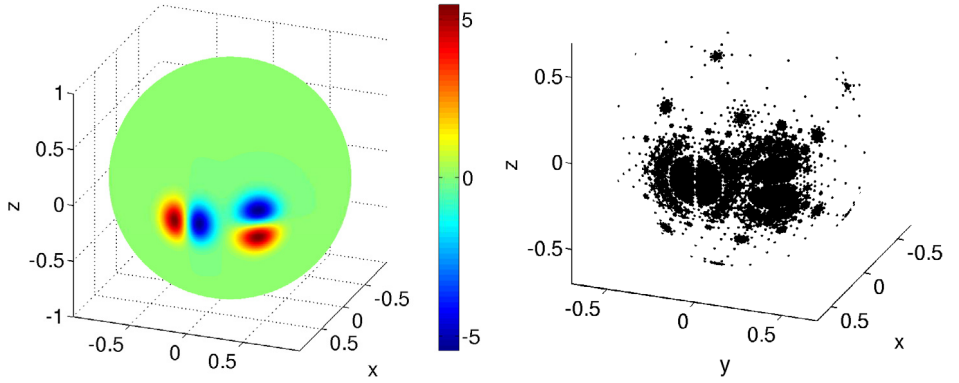

Fig. 5. Approximation of the surface divergence operator of test case-2 (left) and its adaptive grid (right).

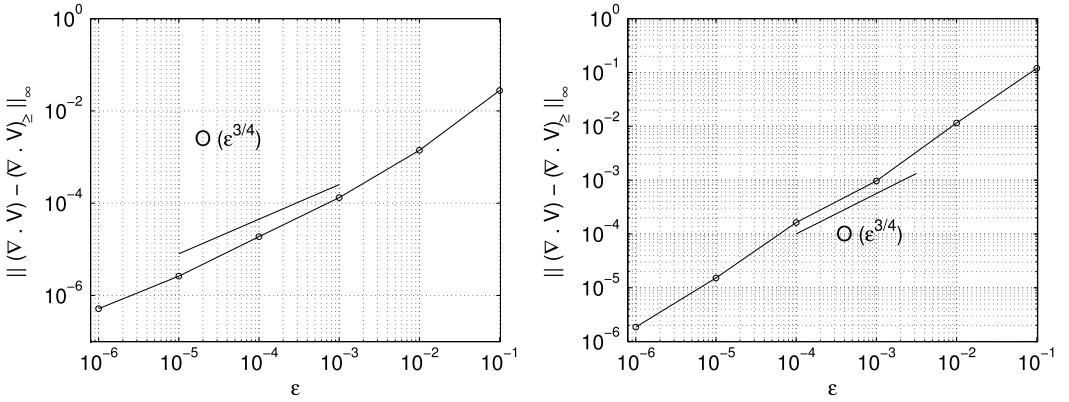

Fig. 6. Relation between ϵ and $\|(\nabla \cdot \vec{\mathbf{V}}) - (\nabla \cdot \vec{\mathbf{V}})_{\geq}\|_{\infty}$ for test case-1 (left) and test case-2 (right).

Section 3. Hence, the approximation of the surface divergence operator is controlled by the tolerance ϵ. Same way, we have also plotted the relation between $\|(\nabla \cdot \vec{\mathbf{V}}) - (\nabla \cdot \vec{\mathbf{V}})_{\geq}\|_{\infty}$ with $N(\epsilon)$ on left of Fig. 7 (test case-1) and right of Fig. 7 (test case-2), which is compared with the theoretical scaling $(N(\epsilon))^{3/2}$.

In order to demonstrate the efficiency of the multi-level adaptive wavelet approximation of the surface divergence operator on spherical geodesic grid, we need to compare the number of grid points used in the adaptive case and non-adaptive case. This can be measured by compression coefficient $\mathcal{C} = \frac{N(\epsilon=0)}{N(\epsilon\neq 0)}$. In Fig. 8 (left) we have plotted the relation between compression coefficient $\mathcal{C}$ and ϵ for test case-1 and the corresponding result for test case-2 is

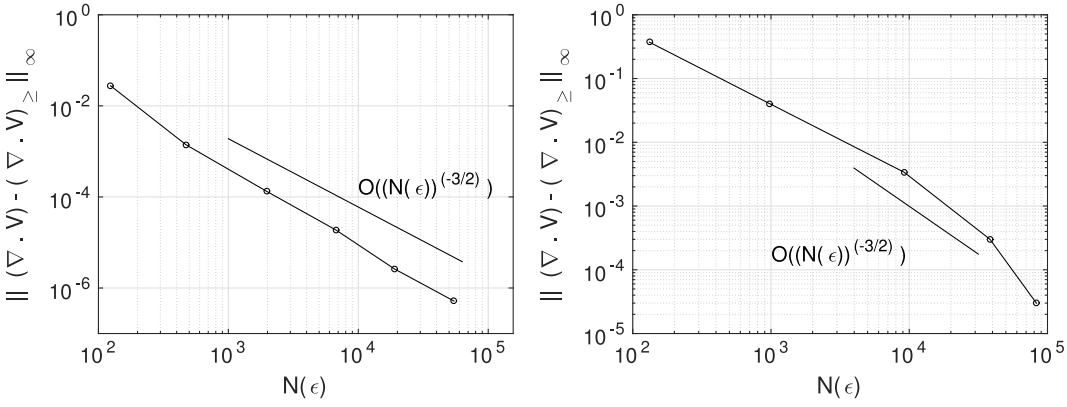

Fig. 7. Relation between $N(\epsilon)$ and $\|(\nabla \cdot \vec{\mathbf{V}}) - (\nabla \cdot \vec{\mathbf{V}})_{\geq}\|_\infty$ for test case-1 (left) and test case-2 (right).

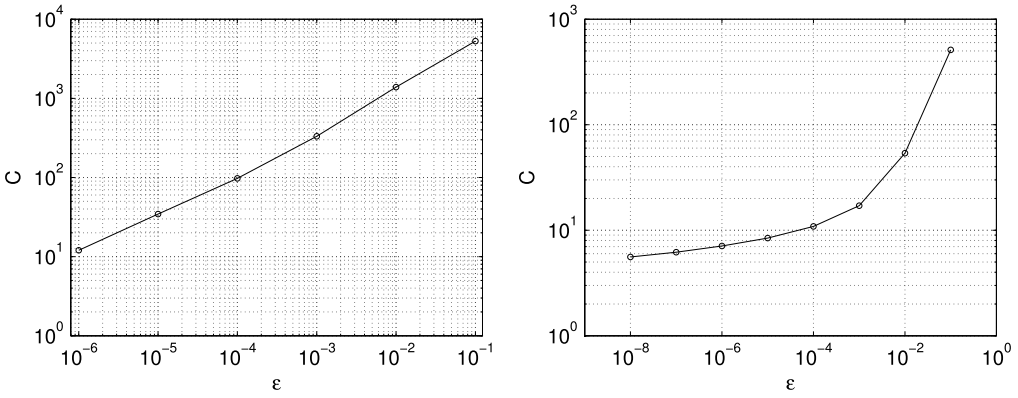

Fig. 8. Relation between compression coefficient ($\mathcal{C}$) and ϵ for test case-1 (left) and test case-2 (right) of surface divergence operator.

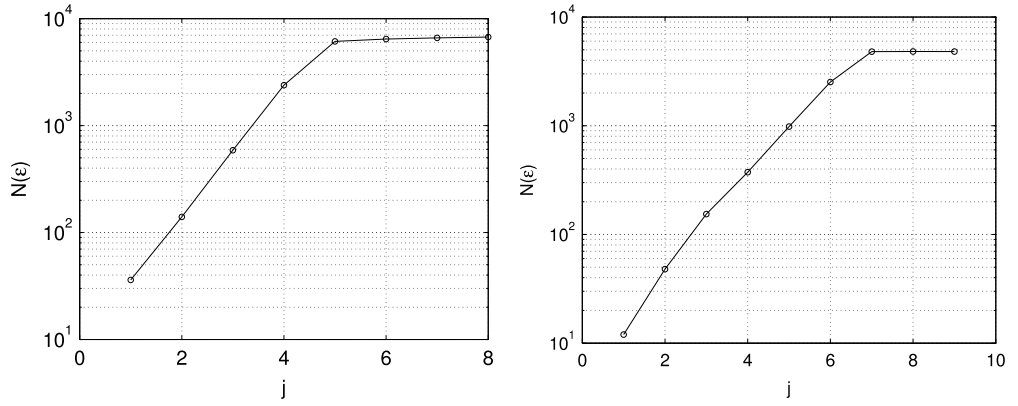

Fig. 9. Relation between $N(\epsilon)$ as a function of number of allowed levels j for test case-1 (left) and test case-2 (right) of surface divergence operator.

presented in Fig. 8 (right). One observes that compression coefficient $\mathcal{C}$ increases when wavelet prescribed threshold parameter (ϵ) increases, which means when ϵ goes to zero, the compression coefficient goes to one, i.e., adaptive algorithm becomes non-adaptive and leads to uniformly refined grids.

We emphasize that the multi-level approach is essential for an efficient adaptive algorithm for fixed levels of resolution j, here we check that $j = 7$ level is sufficient to fully resolve the test functions. This is confirmed in Fig. 9 (left) test case-1 and Fig. 9 (right) test case-2, which shows that the number of active points does not increase when we allow more than $j = 5$ level in test case-1 and $j = 7$ in test case-2.

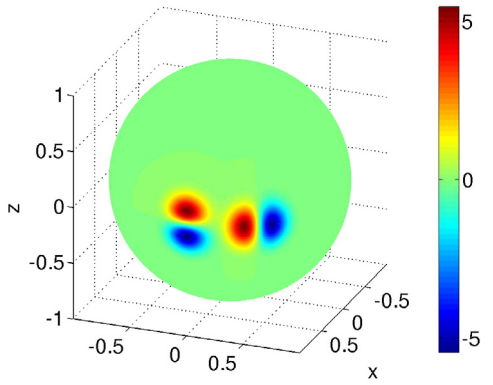

Fig. 10. Approximation of scalar-valued surface curl operator for test case-2.

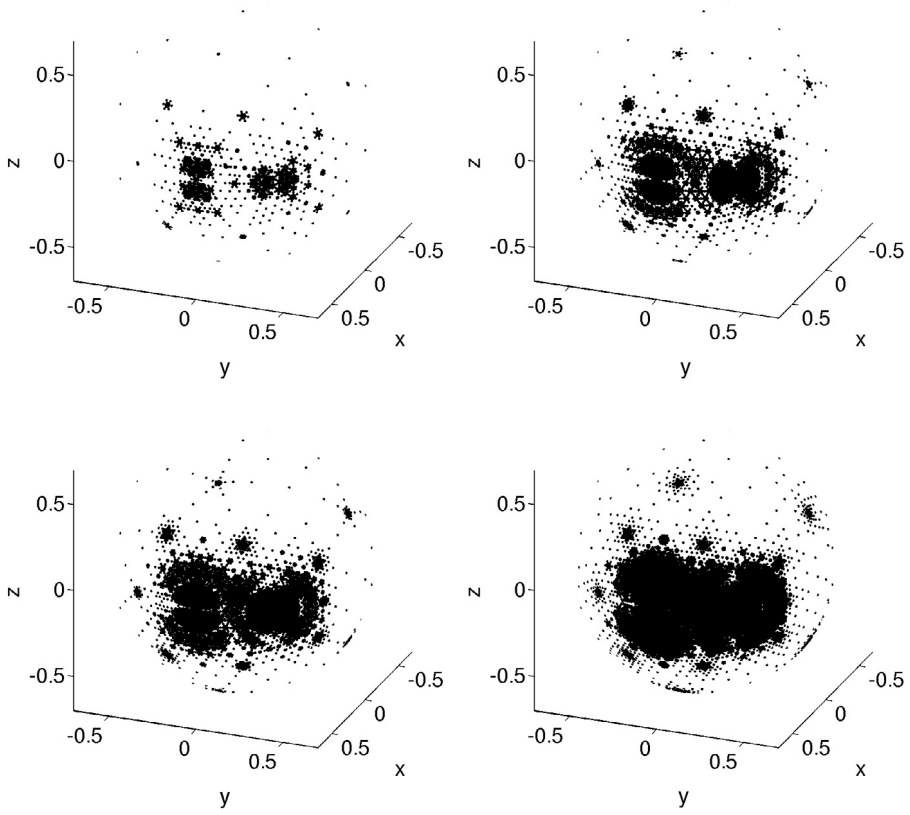

Fig. 11. Adaptive computational grid of the approximation of the scalar-valued surface curl operator at different ϵ (top left $\epsilon = 10^{-1}$, top right $\epsilon = 10^{-2}$, bottom left $\epsilon = 10^{-3}$ and bottom right $\epsilon = 10^{-4}$).

4.2. Adaptive approximation of the scalar-valued surface curl operator

The approximation of scalar-valued surface curl operator of test case-1 is shown in Fig. 10 and its adaptive computational grid $(\vec{\mathbf{K}} \cdot \vec{\nabla} \times \vec{\mathbf{V}})_{\geq}(p)$ is presented in Fig. 11 for different ϵ (top left $\epsilon = 10^{-1}$, top right $\epsilon = 10^{-2}$, bottom left $\epsilon = 10^{-3}$ and bottom right $\epsilon = 10^{-4}$). Hence the grid is fine only in regions where the function has a strong gradient. Therefore, the adaptive grid clearly reflects the structure of the approximation.

We have plotted the relation between $\|(\vec{\mathbf{K}} \cdot \vec{\nabla} \times \vec{\mathbf{V}}) - (\vec{\mathbf{K}} \cdot \vec{\nabla} \times \vec{\mathbf{V}})_{\geq}\|_{\infty}$ with ϵ in Fig. 12 (test case-1 and test case-2). Furthermore, the relation between $\|(\vec{\mathbf{K}} \cdot \vec{\nabla} \times \vec{\mathbf{V}}) - (\vec{\mathbf{K}} \cdot \vec{\nabla} \times \vec{\mathbf{V}})_{\geq}\|_{\infty}$ and $N(\epsilon)$ is represented on left of Fig. 13 (test case-1) and right of Fig. 13 (test case-2) respectively.

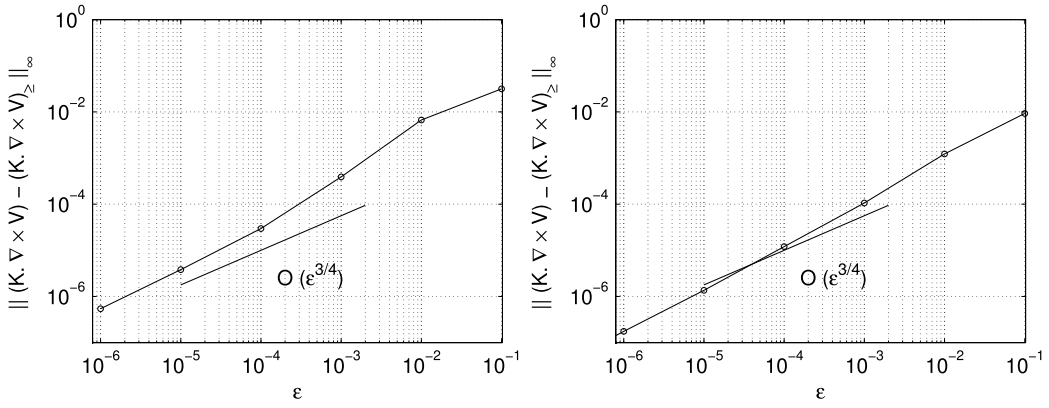

Fig. 12. Relation between ϵ and $\|(\vec{\mathbf{K}} \cdot \vec{\nabla} \times \vec{\mathbf{V}}) - (\vec{\mathbf{K}} \cdot \vec{\nabla} \times \vec{\mathbf{V}})_{\geq}\|_{\infty}$ for test case-1 (left) and test case-2 (right).

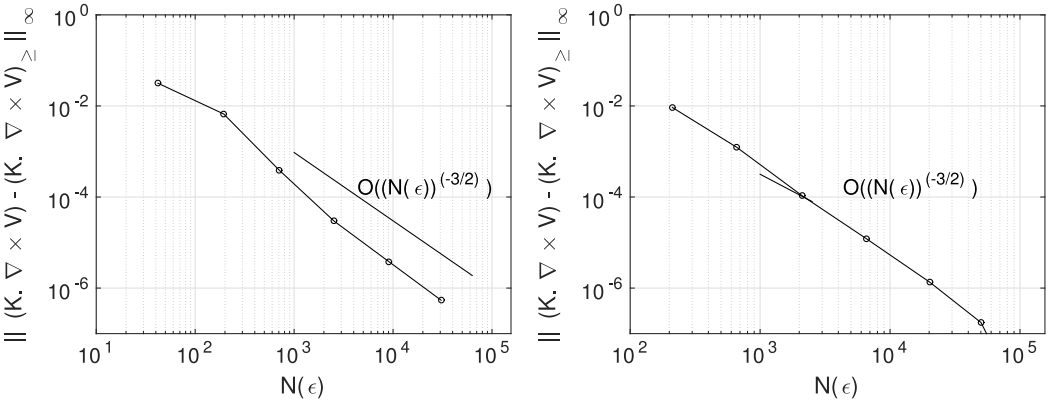

Fig. 13. Relation between $N(\epsilon)$ and $\|(\vec{\mathbf{K}} \cdot \vec{\nabla} \times \vec{\mathbf{V}}) - (\vec{\mathbf{K}} \cdot \vec{\nabla} \times \vec{\mathbf{V}})_{\geq}\|_{\infty}$ for test case-1 (left) and test case-2 (right).

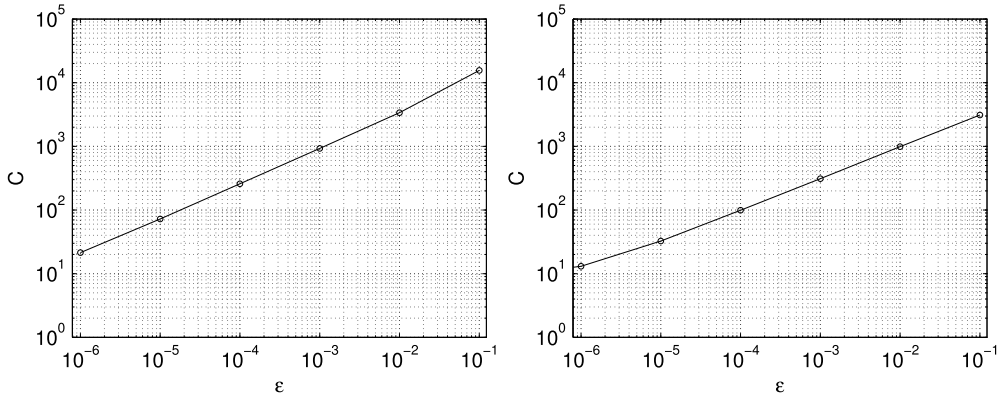

Fig. 14. Relation between compression coefficient ($\mathcal{C}$) and ϵ for test case-1 (left) and test case-2 (right) of scalar-valued surface curl operator.

In the same way to demonstrate the efficiency of the multi-level adaptive wavelet approximation of the scalar-valued surface curl operator on spherical geodesic grid we need to compare the number of grid points used in the adaptive case and nonadaptive case. We have plotted the relation between compression coefficient $\mathcal{C}$ and ϵ for test case-1 in Fig. 14 (left) and test case-2 in Fig. 14 (right).

Fig. 15 represents the relation between j and $N(\epsilon)$, which represents progressive grid adaptation procedure continues adding one by one level until it reaches a steady state where number of active grid points $N(\epsilon)$ does stagnate. Fig. 15 (left) shows that there is a steep increase in number of active grid points with the level of resolution

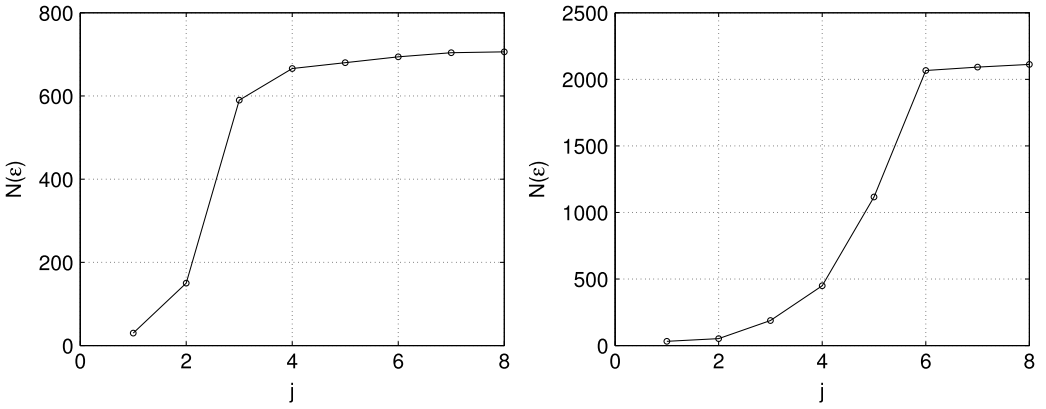

Fig. 15. Relation between $N(\epsilon)$ as a function of number of allowed levels j for test case-1 (left) and test case-2 (right) of scalar-valued surface curl operator.

from $j = 1$ to $j = 4$ and then it slowly plateaus from $j = 4$ onwards and did not increase further from $j = 6$. Fig. 15 (right) shows that there is sigmoidal behavior between $N(\epsilon)$ and j. That is, the number of active grid points increase with the increase of level of resolution from $j = 1$ to $j = 6$ and beyond $j = 6$ it is almost stationary.

4.3. Adaptive solution of advection test cases

Advection processes are of paramount importance in atmospheric numerical modeling. Since the fluid motions on all scales are dominated by the advection process the accurate and efficient numerical solution of the advection problem determines the overall accuracy of the ocean or atmosphere simulation. In order to illustrate the accuracy and efficiency of the proposed approximation of surface divergence operator, we consider dynamic grid adaptation for localized solution of two advection problems: (1) solid body rotation of a cosine bell, (2) deformational (divergent) flow on the sphere.

When solving the evolution equations an additional criterion for grid adaptation should be added. The computational grid should consist of grid points associated with wavelets whose coefficients are significant or that could become significant in one time step. In other words, at any instant in time, the computational grid should consist of the $N(\epsilon)$ significant grid points plus those grid points in an adjacent zone [25] in both position and scale that could become significant in one time step. This allows for development of details on finer scales such as shock and strong gradient. Furthermore, we have all the ingredients necessary to construct a dynamically adaptive algorithm for the solution of evolution problems on the sphere. The three basic steps are as follows:

1. Knowing the solution $u_{\geq}(t)$ on the adaptive grid, we compute the values of wavelet coefficients corresponding to each component of the solution using the fast wavelet transform. For a given threshold ϵ. we update $\mathcal{S}_{\geq}^{t+\Delta t}$ based on the magnitude of wavelet coefficients. We also add an adjacent zone [25] to the significant coefficients to allow for the change in the solution during one time step.
2. If there is no change between computational grids $\mathcal{S}_{\geq}^{t}$ and $\mathcal{S}_{\geq}^{t+\Delta t}$, we go directly to next step. Otherwise we interpolate the values of the solution at the collocation points $\mathcal{S}_{\geq}^{t+\Delta t}$, which are not included in $\mathcal{S}_{\geq}^{t}$.
3. We integrate the resulting system of ordinary differential equations in time (e.g. using Runge–Kutta) to obtain new values to $u_{\geq}(t + \Delta t)$ at positions on adaptive grid $\mathcal{S}_{\geq}^{t+\Delta t}$, and go back to step 1.

With these three steps the grid of collocation points is dynamically adapted in time and follows the local structures that appear in the solution. Note that by omitting wavelets with coefficients below a threshold parameter we automatically control the error of approximation. The smaller ϵ is chosen to be, the smaller the error of the solution is. Thus the second generation wavelet based method has another important feature: active control of the accuracy of the solution.

The objective of this paper is to propose multi-level wavelet approximation of differential operators and using multi-level wavelet approximation of surface divergence operator to solve advection equations on the spherical geodesic grid. Specifically in advection equation, we have demonstrated the computational grid and associated wavelets are very efficiently adapted to the local structure of the solution in order to resolve sharp transition regions.

In order to verify the efficiency and accuracy of grid adaption in an advection process, we have used fourth-order Runge–Kutta method with time step $\Delta t = 10^{-4}$. But many powerful methods have been developed for efficient treatment in the design of an atmospheric model, i.e., exponential propagation method [9] and stiffly stable Krylov time integration technique [15]. Improved spherical wavelet based time integration schemes will be developed in our future work.

4.3.1. Advection of the cosine bell

In this case a cosine bell is advected once around the sphere, which is a standard test case for any numerical scheme considered for climate or weather modeling. The case was suggested by Williamson [47] to simulate the advection of a height field, $u(\theta, \phi)$ on the surface of a sphere at an angle α which is the angle between the axis of solid-body rotation and the coordinate axis of spherical coordinate system. Using adaptive wavelet collocation method [25], the partial differential equation to be solved is the spherical advection equation, which in spherical coordinates is given by

$$\frac{\partial u}{\partial t} + \nabla \cdot (u\mathbf{V}) = 0, \tag{27}$$

where $t \in [0, T]$ is the time and T is the ending time of the simulation, and the advecting wind field is given by $\mathbf{v} = (v_1, v_2)$

$$\begin{aligned} v_1 &= u_0 \left[\cos(\phi)\cos(\alpha) + \sin(\phi)\cos\left(\theta + \frac{3\pi}{2}\right)\sin(\alpha) \right], \\ v_2 &= u_0 \sin\left(\theta + \frac{3\pi}{2}\right)\sin(\alpha), \end{aligned} \tag{28}$$

where u_0 is the advection speed, here we set u_0 so that the rotation period is equal to one. Further, (27) can be written as

$$\frac{\partial u}{\partial t} = -\nabla \cdot (u\mathbf{V}). \tag{29}$$

The initial cosine bell test pattern that is to be advected is given by,

$$u(\theta, \phi) = \begin{cases} \frac{1}{2}\left[1 + \cos(\pi r/R)\right] & \text{if } r < R, \\ 0 & \text{if } r \geq R, \end{cases} \tag{30}$$

where $R = a/3$ and $r = a \arccos[\sin(\phi_c)\sin(\phi) + \cos(\phi_c)\cos(\phi)\cos(\theta - \theta_c)]$, which is the geodesic distance between (ϕ, θ) and the center $(\phi_c, \theta_c) = (0, 0)$. The initial conditions are chosen such that $\alpha = \frac{\pi}{2} - 0.05$ (this is the most unfavorable case for latitude–longitude grids). The exact solution of the advection equation at any time step is simply a translation of the initial condition, since the solid-body rotation moves the cosine bell around the globe without any shape deformation.

The initial cosine bell is plotted in Fig. 16 (left) and its associated adaptive grid is plotted in Fig. 16 (right). Note that this is also the exact solution after one orbit on the non-rotating sphere. Fig. 17 shows the error convergence as a function of tolerance ϵ and as a function of actual number of grid points $N(\epsilon)$ for the solution of advection of cosine bell, where the pointwise L_∞ error of the solutions at the final time of integration is shown. Further, Fig. 17 (left) clearly indicates the convergence of the numerical method with the decrease of ϵ. Thus prescribing the value of ϵ we can actively control the accuracy of the solution.

Fig. 18 (left) shows the time evolution of the total number of collocation points or, effectively, active wavelets as a function of time. We see that the average number of gridpoints is roughly constant (about 16 times compression). Since the solid-body rotation moves the cosine bell around the sphere without any shape deformation, this resulted in an approximate constant of the number of grid points. Further, to get a better idea of how the adaptive grid tracks regions of sharp transition, we have plotted the relation between level the j and the number of active grid points $N(\epsilon)$ in Fig. 18 (right). This figure shows that we need only up to level $j = 7$ because for $j > 7$ there is no change in the number of active points for the range of tolerances considered here.

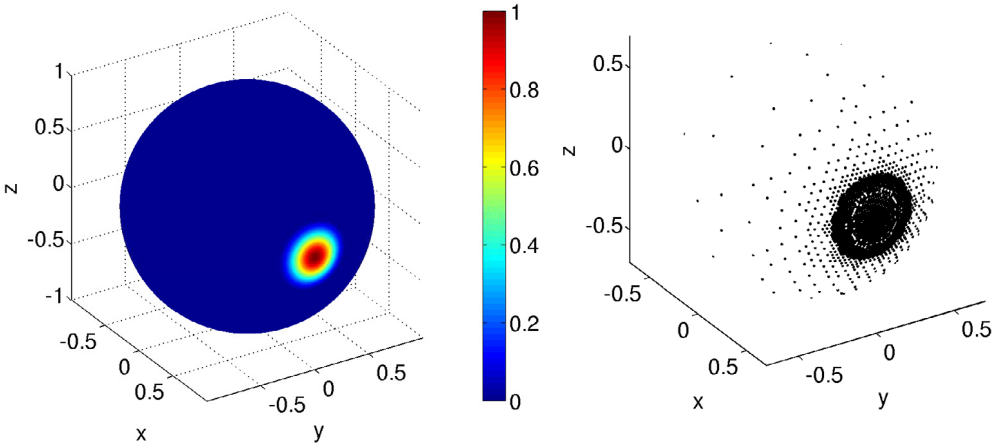

Fig. 16. Cosine bell initial conditions and exact solution after one orbit on a non-rotating sphere (left) and its associated adaptive grid (right).

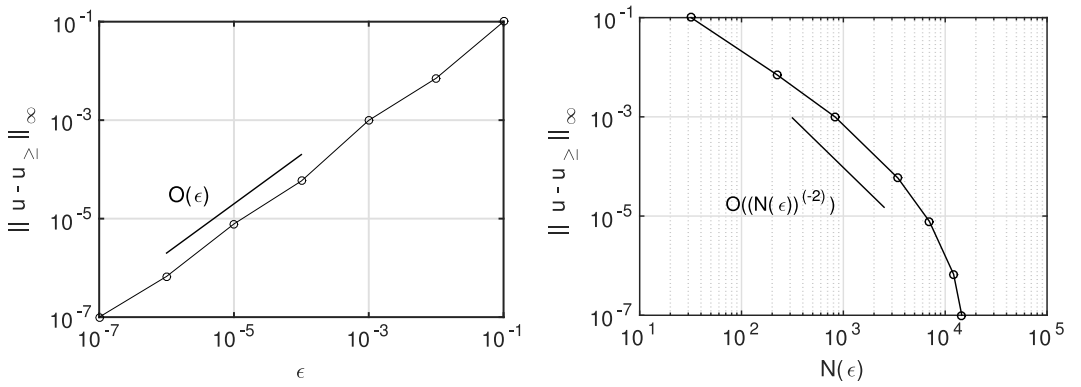

Fig. 17. Convergence error as a function of tolerance ϵ (left) and as a function of actual number of grid points $N(\epsilon)$ in the calculation (right) for the solution of advection of cosine bell.

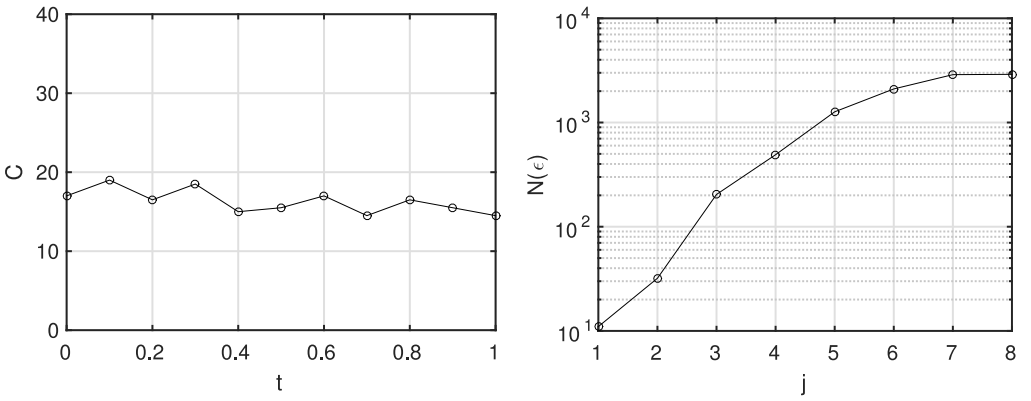

Fig. 18. Time evolution of the compression coefficient $\mathcal{C}$ (left), and relation between the level of resolution j with number of active grid points $N(\epsilon)$ for the solution of advection of cosine bell.

4.3.2. Deformational (divergent) flow

The divergent flow is specifically aimed to solve many global transport schemes which is very challenging in the flow environment. The simplest possible form of the advection scheme was presented and discussed in Section 4.3.1. Now we consider a test case consisting of highly deforming divergent wind field along with initial trace profile of

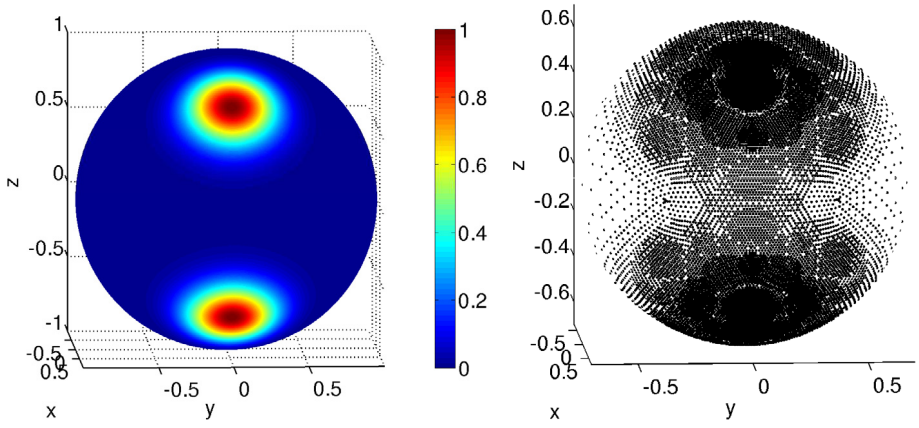

Fig. 19. Initial scalar field $h(t = 0)$ and its adaptive grid.

Gaussian hills. In the absence of sources and/or sinks, the Eulerian form of the mass continuity equation and tracer conservation equation can be written as follows

$$\begin{aligned} &\frac{\partial \rho}{\partial t} + \nabla \cdot (\rho \mathbf{V}) = 0, \\ &\frac{\partial (\rho h)}{\partial t} + \nabla \cdot (\rho h \mathbf{V}) = 0, \end{aligned} \tag{31}$$

respectively, where ρ is the fluid density and h is the tracer concentration (or mixing ratio) per unit mass so that $h\rho$ may be interpreted as the tracer density, $\mathbf{V}$ is the flow velocity vector, which is defined by,

$$\begin{aligned} v_1(\theta, \phi, t) &= -\sin^2(\theta/2)\sin(2\phi)\cos^2(\phi)\cos(\pi t), \\ v_2(\theta, \phi, t) &= \frac{1}{2}\sin(\theta)\cos^3(\phi)\cos(\pi t). \end{aligned} \tag{32}$$

Here cosine-bells as the initial scalar field which is used by Nair and Lauritzen [27], where the cosine-bells are defined by

$$h_i(\theta, \phi) = h_{\max} \exp\left[-b_0\{(x - x_i)^2 + (y - y_i)^2 + (z - z_i)^2\}\right], \tag{33}$$

where $h_{\max} = 1$ is the height [19] of the Gaussian hill and $b_0 = 12$ defines the width. (x, y, z) are the 3D absolute Cartesian coordinates corresponding to the spherical (θ, ϕ) coordinates

$$(x, y, z) = (a\cos\phi\cos\theta, a\cos\phi\sin\theta, a\sin\phi),$$

where radius $a = 1$ (unit sphere). The center of the Gaussian distribution (x_i, y_i, z_i) can be specified in terms of (θ_i, ϕ_i), such that $\theta_1 = -\pi/2, \theta_2 = \pi/2, \phi_1 = 0$ and $\phi_2 = 0$. Finally the cosine bells created two Gaussian hills for initial scalar distribution h as the sum of two fields h_1 and h_2.

$$h(\theta, \phi) = h_1(\theta, \phi) + h_2(\theta, \phi). \tag{34}$$

Here we are solving coupled system of Eq. (31) for air density and tracer density for $\rho(t = 0) = 1$. In Fig. 19 (left), we have plotted the initial condition Eq. (34) of the Gaussian distributions (cosine-bells) and the adaptive grid refinement is plotted in Fig. 19 (right), which is also exact solution for after one rotation.

Using AWCM, we solve these equations and compare this to the exact solution (same as the initial condition) in Fig. 19. Moreover, Fig. 20 shows the convergence of L_∞ error at various resolutions of after one rotation.

5. Conclusion

A new adaptive multi-level approximation of surface divergence and scalar-valued surface curl operators on a recursively refined spherical geodesic grid is developed. Since computation of differential operators is necessary for

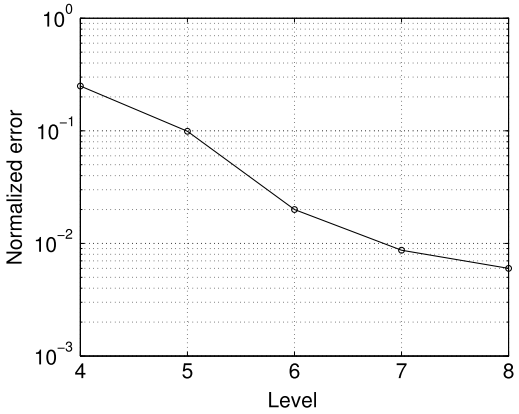

Fig. 20. Convergence of the normalized errors at different levels of resolution.

many applications in data analysis and in the numerical simulation of PDEs on the sphere, this efficient and accurate new technique should be practically useful. Moreover, this approximation technique is more useful in capturing, identifying, and analyzing local structure than any other traditional methods. Furthermore, these approximation operators based on these formulas hold in any coordinates system because they involve only geometrical quantities such as length, area, and volumes and use coordinate invariant component of the vectors. Thus the strength of this approximation scheme is that it can be extended easily to other curved manifolds by considering appropriate coarse approximation to the desired manifold. The numerical results are verified by considering the localized test function proposed in [17] (test case-1) and a Gaussian function (test case-2) on the sphere. Moreover, we also use the multi-level approximation of surface divergence operator in an adaptive wavelet collocation method to solve advection equations. Thus, the strength of this adaptive approximation technique is that it can be applied in atmospheric and geophysical simulation problems, computational fluid dynamics and turbulence flow while retaining the freedom and flexibility.

Acknowledgments

This research work was supported by Department of Science and Technology, India, under the Grant No. RP02417. The authors are indebted to the referees whose suggestions and corrections tremendously improved this manuscript.

References

[1] J.P. Antoine, P. Vandergheynst, Wavelets on the n-sphere and related manifolds, J. Math. Phys. 39 (8) (1998) 3987–4008.
[2] J.P. Antoine, P. Vandergheynst, Wavelets on the 2-sphere: a group theoretical approach, Appl. Comput. Harmon. Anal. 7 (1999) 262–291.
[3] P. Baldi, G. Kerkyacharian, D. Marinucci, D. Picard, Asymptotics for spherical needlets, Ann. Statist. 37 (3) (2009) 1150–1171.
[4] R.B. Barreiro, M.P. Hobson, A.N. Lasenby, A.J. Banday, G. Hinshaw, K.M. Gorski, Testing the Gaussianity of the COBE-DMR data with spherical wavelets, Mon. Not. R. Astron. Soc. 318 (2) (2000) 475–481.
[5] R. Behera, M. Mehra, Integration of barotrophic vorticity equation over spherical geodesic grid using multilevel adaptive wavelet collocation method, Appl. Math. Model. 37 (2013) 5215–5226.
[6] R. Behera, M. Mehra, A dynamic adaptive wavelet method for solution of the Schrodinger equation, J. Multiscale Model. 06 (1) (2015) 1450001–1430023.
[7] R. Behera, M. Mehra, N.K.R. Kevlahan, Multilevel approximation of the gradient operator on an adaptive spherical geodesic grid, Adv. Comput. Math. 41 (3) (2015) 663–689.
[8] G. Ben-yu, A spectral method for the voriticity equation on the surface, Math. Comp. 64 (1995) 1067–1079.
[9] C. Clancy, J. Pudykiewicz, On the use of exponential time integration methods in atmospheric models, Tellus A 65 (2013) 1–16.
[10] A. Cohen, I. Daubechies, J.C. Feauveau, Bi-orthogonal bases of compactly supported wavelets, Comm. Pure Appl. Math. 45 (485) (1992).
[11] I. Daubechies, Ten Lectures on Wavelets, SIAM, 1992.
[12] I. Daubechies, Orthogonal bases of compactly supported wavelet II. Variation on a theme, SIAM J. Math. Anal. 24 (2) (1993) 499–519.
[13] D.L. Donoho, Interpolating wavelet transforms. Technical Report 408, Department of Statistics, Stanford University, 1992.
[14] N. Dyn, D. Levin, J. Gregory, A butterfly subdivision scheme for surface interpolation with tension control, Trans. Graph. 9 (2) (1990) 160–169.
[15] W.S. Edwards, L.S. Tuckerman, R.A. Friesner, D.C. Sorensen, Krylov methods for the incompressible Navier–Stokes equations, J. Comput. Phys. 110 (1994) 82–102.

[16] W. Freeden, U. Windheuser, Combined spherical harmonic and wavelet expansion a future concept in the earths gravitational determination, Appl. Comput. Harmon. Anal. 4 (1997) 1–37.
[17] R. Heikes, D.A. Randall, Numerical integration of the shallow-water equations on a twisted icosahedral grid. part: Basic design and results of test, Mon. Weather Rev. 123 (1995) 1862–1880.
[18] M. Holschneider, Continuous wavelet transforms on the sphere, J. Math. Phys. 37 (1996) 4156–4165.
[19] M.N. Levy, R.D. Nair, H.M. Tufo, High-order Galerkin method for scalable global atmospheric models, Comput. Geosci. 33 (2007) 33 (2007) 1022–1035.
[20] D. Marinucci, D. Pietrobon, A. Balbi, P. Baldi, P. Cabella, G. Kerkyacharian, P. Natoli, D. Picard, N. Vittorio, Spherical needlets for cosmic microwave background data analysis, Mon. Not. R. Astron. Soc. 383 (2) (2008) 539.
[21] Y. Masuda, H. Ohnishi, An integration scheme of the primitive equation model with a icosahedral-hexagonal grid system and its application to the shallow water equations, in: T. Matsuno (Ed.), Short and Medium Range Numerical Weather Predication, Meteorological Society of Japan, 1986, pp. 317–326.
[22] J.D. McEwen, A.M.M. Scaife, Simulating full-sky interferometric observations, Mon. Not. R. Astron. Soc. 389 (3) (2008) 1163–1178.
[23] J.D. McEwen, Y. Wiaux, D.M. Eyers, Data compression on the sphere, Astron. Astrophys. 531 (2011).
[24] M. Mehra, N.K.R. Kevlahan, An adaptive multilevel wavelet solver for elliptic equations on an optimal spherical geodesic grid, SIAM J. Sci. Comput. 30 (6) (2008) 3073–3086.
[25] M. Mehra, N.K.R. Kevlahan, An adaptive wavelet collocation method for the solution of partial differential equation on the sphere, J. Comput. Phys. 227 (2008) 5610–5632.
[26] M. Meyer, M. Desbrun, P. Schroder, A. Barr, Discrete differential geometry operator for triangulated 2-manifolds, in: Visualization and Mathematics III, 2002, pp. 35–57.
[27] R.D. Nair, P.H. Lauritzen, A class of deformational flow test cases for linear transport problems on the sphere, J. Comput. Phys. (2010) http://dx.doi.org/10.1016/j.jcp.2010.08.014.
[28] F.J. Narcowich, P. Petrushev, J.D. Ward, Localized tight frames on spheres, SIAM J. Math. Anal. 38 (2) (2006) 574–594.
[29] F.J. Narcowich, J.D. Ward, Non-stationary wavelets on the m-sphere for scattered data, Appl. Comput. Harmon. Anal. 3 (1996) 324–336.
[30] J.A. Pudykiewicz, Numerical solution of the reaction-advection-diffusion equation on the sphere, J. Comput. Phys. 213 (2006) 358–390.
[31] J.A. Pudykiewicz, On numerical solution of the shallow water equations with chemical reactions on icosahedral geodesic grid, J. Comput. Phys. 230 (2011) 1956–1991.
[32] T.D. Ringler, D.A. Randall, A potential enstrophy and energy conserving numerical scheme for solution of the shallow-water equations on a geodesic grid, Mon. Weather Rev. 130 (2001) 1397–1410.
[33] O.V. Roussel, K. Schneider, Coherent vortex simulation of weakly compressible turbulent mixing layers using adaptive multiresolution methods, J. Comput. Phys. 229 (2010) 2267–2286.
[34] O.V. Roussel, K. Schneider, A. Tsigulin, H. Bockhorn, A conservative fully adaptive multiresolution algorithm for parabolic PDEs, J. Comput. Phys. 188 (2003) 493–523.
[35] R. Sadourny, A. Akakawa, Y. Mintz, Integration of the nondivergent barotropic vorticity equation with an icosahedral-hexagonal grid for the sphere, Mon. Weather Rev. 96 (1968) 351–356.
[36] P. Schroder, W. Sweldens, Spherical wavelets: Efficiently representing functions on the sphere, in: Proceedings of the 22nd Annual Conference on Computer Graphics and Interactive Techniques, 1995, pp. 161–172.
[37] J.L. Starck, Y. Moudden, P. Abrial, M. Nguyen, Wavelets, ridgelets and curvelets on the sphere, Astron. Astrophys. 446 (2006) 1191–1204.
[38] W. Sweldens, The lifting scheme: A custom-design construction of biorthogonal wavelets, Appl. Comput. Harmon. Anal. 3 (2) (1996) 186–200.
[39] W. Sweldens, The lifting scheme: A construction of second generation wavelets, SIAM J. Math. Anal. 2 (29) (1998) 511–546.
[40] H. Tomita, M. Tsugawa, M. Satoh, K. Goto, Shallow water model on a modified icosahedral geodesic grid by using spring dynamics, J. Comput. Phys. 174 (2001) 579–613.
[41] O.V. Vasilyev, Solving multi-dimensional evolution problems with localized structure using second generation wavelets, Int. J. Comput. Fluid Dyn. 17 (2) (2003) 151–168.
[42] O.V. Vasilyev, C. Bowman, Second generation wavelet collocation method for the solution of partial differential equations, J. Comput. Phys. 165 (2000) 660–693.
[43] O.V. Vasilyev, S. Paolucci, A dynamically adaptive multilevel wavelet collocation method for solving partial differential equations in a finite domain, J. Comput. Phys. 125 (111) (1996) 498–512.
[44] O.V. Vasilyev, S. paolucci, M. Sen, A multilevel wavelet collocation method for solving partial differential, J. Comput. Phys. 120 (1995) 33–47.
[45] Y. Wiaux, J.D. McEwen, P. Vandergheynst, O. Blanc, Exact reconstruction with directional wavelets on the sphere, Mon. Not. R. Astron. Soc. 388 (2) (2008) 770–788.
[46] D.L. Williamson, Integration of the barotrophic vorticity equation on a spherical geodesic grid, Tellus 4 (1968) 642–653.
[47] D.L. Williamson, J.B. Drake, J.J. Hack, R. Jacob, P.N. Swarztrauber, A standard test set for numerical approximations to the shallow water equations in spherical geometry, J. Comput. Phys. 102 (1992) 211–224.